This is a preprint, the final version is subject to change, of the American Mineralogist (MSA)
Cite as Authors (Year) Title. American Mineralogist, in press.
(DOI will not work until issue is live.) DOI: http://dx.doi.org/10.2138/am-2017-6011

Revision 1

The relationship between color change and pleochroism in a chromium-doped synthetic chrysoberyl (*var* alexandrite): Spectroscopic analysis and colorimetric parameters

Ziyin Sun[1], Aaron C. Palke[2,*], Jonathan Muyal[1], and Robison McMurtry[1]

[1]Gemological Institute of America, 5345 Armada Dr, Carlsbad, California, 92008, United States

[2]University of Queensland and Queensland Museum, Brisbane, Australia,

*aaronpalke@gmail.com

Abstract

Pleochroism plays an important role in determining the face-up visual color appearance of faceted, optically anisotropic (non-cubic) gemstones. One area that has received little attention is the interplay between pleochroism and the so-called Alexandrite effect wherein the perceived color of a mineral changes with different lighting conditions (i.e. daylight vs. incandescent light). In this article we have collected ultraviolet/visible/near-infrared (UV-Vis-NIR) spectra of a gem-quality, synthetic Cr-bearing chrysoberyl crystal along its three crystallographic axes. We use these spectra to calculate the color and to quantify the color change that would be observed in a wafer or faceted gemstone in any orientation and for any prescribed path length of light between 1 and 25 mm. We describe the method used to perform these calculations and give an overview of color science and color space as it pertains to mineralogy and gemology. The data collected here are used to predict the optimum orientation for a wafer or a faceted alexandrite gemstone to produce the maximum color change sensation between daylight and an incandescent light source.

We find that a wafer oriented with the unpolarized light-path-length perpendicular to the a-axis exhibits the strongest color change but that the color change is weaker parallel to the a-axis. Pleochroism in a faceted stone will mix light travelling in different directions. This relaxes requirements to orient a stone along the "best" direction, but it is still found that stones cut with their table to culet direction oriented perpendicular to the a-axis show the best color-change while orientation parallel to the a-axis produces weaker color change. Nonetheless, there is a wide range of "acceptable" orientations and no single "best" direction for a facetted gemstone. The results of this study demonstrate the complex nature of color in minerals and shed light on the intricate interplay between a number of factors including pleochroism, lighting conditions, light path length through a transparent sample, and chromophore concentrations. The use of the techniques outlined here can lead to a better understanding of the color sciences in the mineral world in general.

Keywords: Alexandrite, alexandrite effect, pleochroism, Usambara effect, visible spectrocopy, colorimetry

Introduction

Color is an invaluable tool in the mineralogical sciences. As useful as it is as an aid in mineral identification, color can also help to provide a rough idea of the chemistry of many minerals and can even elucidate the geological history of a mineral in many cases. For instance, brown and pink coloration in diamond can be an indicator of plastic deformation (Collins 1982; Smith et al. 2010; Howell et al. 2015) pink to yellow color can be induced in tourmaline by natural or artificial irradiation (Reinitz and Rossman 1988; Krambrock et al 2004). In the laboratory, the color of a mineral is usually interrogated using ultraviolet-visible (UV-Vis)

absorption spectroscopy (e.g. Rossman 2014). UV-Vis spectroscopy, furthermore, is useful as well for measuring site occupancies and oxidation states of transition metals in many minerals (Geiger et al. 2000; Fregola et al. 2014; Bosi et al. 2015). Visible and near-infrared absorption spectroscopy are also becoming increasingly useful in remote sensing and hyperspectral imaging (Kozak et al. 2004; Ling et al. 2008; Sobron et al. 2014; Turner et al 2016). Nonetheless, the correlation between visible absorption and color is not always so straightforward.

In fact, Halvorsen and Jensen (1997), Liu et al. (1999b), Pearson and Hoover (2003), and Halvorsen (2006) have shown that the color of some unusual tourmalines from Usambara, Tanzania varies significantly depending on the path length of light through the material. Mineralogists and gemologists know this phenomenon as the Usambara effect although it was recognized previously by color scientists in materials such as chlorophyll (Bamford, 1977; Nassau, 1983). The same effect can also be seen with variations in chromophore concentration. This tourmaline from Usambara also exhibited a distinct change in color under different lighting conditions (i.e. daylight vs. incandescent light). This phenomenon is often called the "alexandrite effect" after the Cr-bearing variety of chrysoberyl (White, et al., 1967; Troup, 1969; Gübelin and Schmetzer, 1980, 1982; Liu et al., 1994, 1999a; Schmetzer et al., 2013, Sun et al., 2015). Fine alexandrite specimens will appear green to blue in daylight, and purple to red in incandescent light (in this contribution we will often refer to D65 or A illumination roughly corresponding to daylight or incandescent lighting, respectively). These two types of lighting (incandescent and daylight) emphasize the transmission of one or the other of these colors. Selective absorption of visible light by Cr^{3+} creates different colors in alexandrite by producing two transmission "windows" in the red and blue/green portions of the visible spectrum (Farrell and Newnham 1965; Hassan and El-Rakhawy 1974; Powell et al. 1985; Garcia-Lastra et al. 2006; Schmetzer

and Bosshart 2010; Schmetzer and Malsy 2011; Schmetzer 2012; Schmetzer et al. 2012, 2013; Witthayarat et al. 2014).

Sun et al. (2015) recently explored the relationship between light path length and the alexandrite effect by calculating the color for a Cr- and V-bearing pyrope garnet at varying path lengths. One can additionally introduce another complicating factor into the problem of color in minerals by considering the effect of pleochroism. Hughes (2014) showed the dramatic affect that pleochroism can have in the observed colors of a faceted, non-cubic gemstones in various orientations. In this contribution we perform a colorimetric analysis of a synthetic Cr-bearing chrysoberyl cuboid (*var.* alexandrite) which is a pleochroic gem material that displays different color sensations under different lighting conditions. We show that the magnitude of the color change in this material depends not only on the path length of light but also on the orientation of the material. We also approximately calculate the appearance of a faceted gem cut out of this material under various orientations to attempt to determine the "best" orientation in which the stone can be cut. The results of this study demonstrate the importance of pleochroism, light path length, and chromophore concentration in understanding and interpreting the significance of observed color in minerals and gems.

Chrysoberyl structure and optical properties

In chrysoberyl Al^{3+} and Be^{2+} occupy octahedral and tetrahedral sites in the crystal structure, respectively (Bragg and Brown 1926); and Cr^{3+} substitutes for Al^{3+} in the octahedral sites. The crystallographic axes a, b and c of chrysoberyl (**Figure 1**) used here are based on the assignment of the structure derivation of Farrell et al. (1963) with lattice parameters a = 9.404 Å, b = 5.476 Å, and c = 4.427 Å (a:b:c = 1.7173 : 1 : 0.8084). The parameters of rhombic unit was

refined to a = 9.407(4) Å, b = 5.4781(5) Å, c = 4.4285(3) Å by Dudka et al. (1985). The orientation of the crystallographic axes relative to the optic axes is illustrated on a diagram in **Figure 1**. In a biaxial crystal, the index of refraction for light varies with its vibration direction. Two unique, mutually perpendicular directions can be located in which the crystal exhibits its greatest and least refractive indices, γ and α, respectively. The third refractive index, which is perpendicular to these two, is β. These three directions are called the three principal vibration axes and commonly symbolized as X, Y and Z (**Figure 1**, Bloss 1961; Hughes 2014). Chrysoberyl is optically biaxial positive with refractive indices: α = 1.746-1.747, β = 1.748-1.750, γ = 1.755-1.758, and a 2V angle = 45°. In this article, we take the principal vibration direction X to be parallel to the crystallographic c-axis, Y parallel to the a-axis, and Z parallel to the b-axis (**Figure 1**, Hurlbut 1971; Cline et al. 1979). Note, however, that other researchers (Schmetzer and Bosshart 2010; Schmetzer and Malsy 2011; Schmetzer 2012, Schmetzer et al. 2012, 2013) analyzing the pleochroic colors in chrysoberyl often use a different orientation with Z parallel to the c-axis, Y parallel to the b-axis, and X parallel to the a-axis. This is based on the structure derivation of a : b : c = 0.4707 : 1 : 0.5823 from Bragg and Brown (1926).

Materials and methods

Samples

A Czochralski-grown synthetic alexandrite crystal (Bukin et al. 1981; Guo et al. 1986, 1987) was cut into a rectangular cuboid (length 3.180 mm, width 2.651 mm and height 2.742 mm). The sides of the cuboid were oriented to be perpendicular to the crystallographic axes using an orienting device described by Thomas et al. (2014). Using a synthetic crystal is necessary to simplify this study. Twinning, inclusions, and inhomogeneity of chromophores in

natural crystals make the behavior of light change unpredictably in different crystallographic directions.

LA-ICP-MS analysis

The chemical composition for the synthetic alexandrite was obtained with a ThermoFisher iCAP Qc ICP-MS coupled with a New Wave Research UP-213 laser ablation unit with a frequency-quintupled Nd:YAG laser (213 nm wavelength) running at 4 ns pulse width. USGS glass standards GSD-1G and GSE-1G were used for external calibration. Ablation was achieved using a 55 μm diameter laser spot size, a fluence of around 10 J/cm^2, and a 7 Hz repetition rate. The samples were internally standardized with ^{27}Al using concentrations obtained from EPMA measurements. We selected four spots in the center of different sides of the cuboid in the same region where the spectroscopic data were collected.

Electron probe microanalysis (EPMA)

The chemical composition of the synthetic alexandrite was also measured at Caltech on a JEOL JXA-8200 electron microprobe with an accelerating voltage of 15 kV and 20 nA current with a beam size of 1 μm. Synthetic oxide or metal standards were used to obtain quantitative analytical results. The relative uncertainties of the element concentrations are about 1.5 %. The only two elements detected were Al and Cr. All other elements analyzed (Na, K, Mn, Ga, Cu, Cr, and Ti) were below the detection limit (generally 0.003 to 0.024 wt.% oxides).

UV-VIS-NIR spectroscopy

Spectra using polarized light were collected with a rotatable polarizer set between the light source and the sample in the 190 to 1100 nm range and spectra using unpolarized light were

132 collected without the polarizer in the 250 to 1000 nm range using a Hitachi U-2910 spectrometer
133 and a 1nm spectral resolution at a scan speed of 400 nm/min.

134 **Color representation with digital photography**

135 The colors of the rectangular cuboid along a, b, and c axes were imaged under both
136 incandescent light and fluorescent light to compare with the calculated color panels. Specific
137 lighting used was (GE LIGHTING 790 HALOGEN Bulb, 25W, 14V, with a color temperature
138 around 2700K, similar to CIE [International Commission on Illumination] illuminant A) and
139 (KINO FLO KF55 F8T5 CE, 8W, which is similar to CIE illuminant F7 which is a reasonable
140 substitute for daylight or CIE illuminant D65, CIE 2004) respectively.Color correction of the
141 images was done by using a Gray Color filter (from CVI Melles Griot) and Adobe bridge
142 software. The color hue differences between images of the cuboid and calculated panels are
143 likely caused by different relative spectral power distribution curves (a measurement that
144 describes the relative intensities of different wavelengths of light in an illuminant), different light
145 temperatures, and the setting of the camera despite efforts to control those variables. The
146 lightness (human visual perception of brightness, see discussion below) differences are caused
147 by our choice of exposure time for the camera. The f-number of the digital camera is f/2.8 and
148 ISO (the measurement of the sensitivity of the image sensor in digital camera) used was 320.

149 **Results and discussion**

150 **Chemical Analysis**

151 The chromium content of the synthetic alexandrite was measured using both Electron
152 Probe MicroAnalysis (EPMA) and Laser Ablation Inductively Coupled Plasma Mass
153 Spectrometry (LA-ICP-MS). The results are shown in **Table 1**. Both methods show good

agreement on the absolute concentration of Cr with an average of 1360 ppm from EPMA and 1368 ppm from LA-ICP-MS. When wt. % BeO is calculated from EPMA measurements assuming a stoichiometric formula of $Be(Al,Cr)_2O_4$ there is a significant deviation from 100 wt.% oxide totals (**Table 1**). The exact nature of this deficiency is unknown. It may be possible that there is some deviation from ideal chrysoberyl stoichiometry in this high-temperature synthetic material as seen for structurally related synthetic $MgAl_2O_4$ spinel (i.e. Erukhimovitch et al. 2015). Our focus here was to measure the chromium concentration in this material and so the possibility of non-stoichiometry in synthetic chrysoberyl is a subject for further study.

Visible Absorption Spectrum Analysis

Unpolarized visible-light spectra of the cuboid were recorded with propagation directions along the three crystallographic axes (**Figure 1**).Polarized light spectra were also collected with the electric vector aligned along the three crystallographic axes. The polarized light spectra were normalized to a 1 mm path length and are shown in **Figure 2**. These spectra are designated as "E||a", "E||b", and "E||c" for polarization along the a-, b-, and c-axes, respectively. The spectra are characterized by two broad absorptions centered at approximately 412-421 nm and 561-594 nm which is typical of Cr^{3+} absorption in oxides and silicate minerals (Anderson 1950; Hassan and El-Rakhawy 1974). The positions of these bands are similar in the three polarization directions although their relative intensities dramatically differ. In addition, the characteristic sharp, low-intensity spin-forbidden Cr^{3+} absorptions are seen at 643, 655, and 679 nm (Hassan and El-Rakhawy 1974).

The unpolarized-light spectra were also collected with the path-length of light along the three crystallographic directions of the alexandrite crystal. The spectra for this material

normalized to a 1 mm path length are shown in **Figure 3**. Spectra are designated as "A-down-a", "A-down-b", and "A-down-c" for unpolarized-light spectra down the a-, b-, and c-axes, respectively.

Using the visible spectra to quantitatively calculate color and to predict the color for samples with longer (or shorter) path lengths, requires accurate correction of the absorption baseline, which, in our instrument, is dominantly produced by reflection of light from the top and bottom surfaces of the cuboid (Sun et al. 2015). This correction was made by subtracting the absorbance value at 800 nm, where there is not expected to be any chromophoric absorption, from values for every other data point along the rest of the spectrum. The resulting "reflection loss corrected" spectra then can be extrapolated to spectra with various path lengths without unnecessarily multiplying the absorption due to reflection loss (Sun et al. 2015).

Brief overview of "color space" and quantitative color analysis

Accurate reproduction and measurement of color has been of paramount interest to many scientific disciplines since even before the digital revolution that allowed almost trivial manipulation of color. The human eye has three types of cone receptors which are responsible for color perception. Each type of cone has its maximum sensitivity at short, medium, or long wavelengths. Fundamentally, any color can be reproduced using three parameters to account for these three basic stimuli. In practice, the three "tristimulus values" employed are mathematical constructs that do not necessarily correspond to distinct colors. One of the most commonly utilized sets of tristimulus values is the CIE XYZ color space (CIE 1931).

Such tristimulus values allow a color to be calculated for a specific object based on the spectrum of light collected from a reflection off of its surface or by transmission through the object:

$$X = \frac{\sum_{380}^{780} S(\lambda) \times \bar{x}(\lambda) \times \Delta\lambda \times T\%(\lambda)}{\sum_{380}^{780} S(\lambda) \times \bar{y}(\lambda) \times \Delta\lambda} \quad (1)$$

$$Y = \frac{\sum_{380}^{780} S(\lambda) \times \bar{y}(\lambda) \times \Delta\lambda \times T\%(\lambda)}{\sum_{380}^{780} S(\lambda) \times \bar{y}(\lambda) \times \Delta\lambda} \quad (2)$$

$$Z = \frac{\sum_{380}^{780} S(\lambda) \times \bar{z}(\lambda) \times \Delta\lambda \times T\%(\lambda)}{\sum_{380}^{780} S(\lambda) \times \bar{y}(\lambda) \times \Delta\lambda} \quad (3)$$

wherein $T\%(\lambda)$ is the percentage of light transmitted through the material at a specific wavelength λ, $s(\lambda)$ is the spectral power distribution of the illuminant used for observation of the color, and $\overline{x}(\lambda)$, $\overline{y}(\lambda)$, and $\overline{z}(\lambda)$ are mathematical functions representing, essentially, the "sensitivity" of each of the tristimulus values to various wavelengths of light. Values for $s(\lambda)$,$\overline{x}(\lambda)$, $\overline{y}(\lambda)$, and $\overline{z}(\lambda)$ can be found in CIE (1931). "$\sum_{380}^{780} \Delta\lambda$ " represents Riemann summation over the visible portion of the electromagnetic spectrum with λ in units of nm. More details of this calculation can be found in CIE (1931) or other works such as Nassau (1983).

Using the unpolarized-light spectra shown in **Figure 3** we can calculate the color that should be seen when viewing the cuboid down each of the three crystallographic axes. The results for illuminants A and D65 (corresponding to incandescent and daylight illumination) are shown in **Figure 4**. Also shown are carefully white-balanced images taken of the cuboid using an incandescent light (A) and a fluorescent light that closely approximates daylight conditions (F7). Overall, the calculated colors closely match the colors documented photographically. The images show the cuboid to be significantly lighter than predicted colors, but this is due simply to our

choice of camera exposure time. The close agreement between calculated and observed colors suggests that our calculations extrapolated to longer path lengths of light should accurately represent the colors that would be seen in such stones.

The major drawback of the CIE XYZ color space for our purposes is that colors are not dispersed in the Cartesian coordinate space based on an even distribution of color sensation. Therefore, the Euclidean distances calculated between various color coordinates cannot be reasonably compared to each other. For this reason, in 1976 the International Commission on Illumination (CIE) developed the CIE L*a*b* color space (**Figure 5**, CIE 1977). In this system colors are dispersed on a circular grid with a* and b* representing the horizontal and vertical Cartesian axes and L* representing displacement perpendicular to the circular a*-b* grid. Different combinations of a* and b* can reproduce different hues while the position of a color coordinate along L* represents the lightness of the color (or conversely the color's darkness). For instance, a purely black color has a L* = 0 while a purely white color has L* = 100. When colors are represented graphically in this system, L* is typically fixed at a certain value and the colors for all a*-b* coordinates are displayed in this circular cross section (**Figure 5**, L* = 25, 50 and 75). The a*-b* coordinates can also be converted to polar coordinates in which the polar angle "h_{ab}" represents the "hue" of a color (i.e. the hue angle) and radial distance "C^*_{ab}" represents the "chroma" or the intensity/saturation of the hue. See CIE (2004) for details on converting CIE XYZ coordinates to the CIE L*a*b* color space.

The utility of the CIE L*a*b* color space lies in the fact that the colors are approximately evenly spaced based on visual color sensation. Therefore, if the Euclidean distance between two color coordinates x1 and y1 is twice that between x2 and y2 then people with normal color vision will perceive the color difference between x1 and y1 to be twice that between x2 and y2. The

CIE L*a*b* system then is ideally suited to quantitatively measure the color difference for minerals and gems which exhibit the color change phenomenon under different illuminants. In this case, the absolute difference between the color under daylight (D65) and incandescent light (A) is determined by:

$$\Delta E^*_{ab} = \sqrt{\Delta a^{*2} + \Delta b^{*2} + \Delta L^{*2}} \quad (4)$$

wherein $\Delta a^* = |a^*_{D65} - a^*_A|$, $\Delta b^* = |b^*_{D65} - b^*_A|$, and $\Delta L^* = |L^*_{D65} - L^*_A|$, where the subscripts "D65" or "A" represent the value of the color coordinate in daylight-equivalent or incandescent lighting, respectively (CIE 1931). Additionally, the hue angle difference (Δh_{ab}) and chroma difference (ΔC^*_{ab}) between the two colors can also be determined:

$$\Delta h_{ab} = |h_{ab,D65} - h_{ab,A}| \quad (5)$$

$$\Delta C^*_{ab} = |C^*_{ab,D65} - C^*_{ab,A}| \quad (6).$$

Using these three values (ΔE^*_{ab}, Δh_{ab} and ΔC^*_{ab}), one can make comparisons between the color change phenomenon observed between different materials or for a single material at various path lengths of light through the material. While there is no single, objective set of criteria by which to determine whether or not a mineral or gem ought to be classified as exhibiting the "color change" phenomenon, the guidelines proposed by various researchers typically require that the values of ΔE^*_{ab}, Δh_{ab}, and/or ΔC^*_{ab} surpass some threshold value or that the color coordinates for the material lie within some certain field when two of these variables are plotted against each other (Liu et al. 1994, 1999a; Schmetzer et al. 2009). In this contribution we will use these three values to describe the color difference of a synthetic alexandrite to quantitatively evaluate the

color change of this material under D65 and A illumination as the path length of light through the material is increased.

The strong pleochroism of alexandrite requires us, additionally, to consider the color change seen in three crystallographic directions through the material. We use UV-Vis-NIR spectra collected along the three crystallographic axes to calculate the color which would be seen with light passing through any direction of the crystal. This information is then used to determine the direction through which the maximum values of ΔE^*_{ab}, Δh_{ab}, and/or ΔC^*_{ab} will be obtained. Approximately considering the effect of pleochroism in a faceted gemstone, we attempt to determine the "best" direction along which this type of synthetic alexandrite ought to be faceted to bring out the best color change.

Calculated color and colorimetric parameter maps of unpolarized light through the alexandrite wafer

The absorption spectrum of light passing through the alexandrite along any crystallographic orientation can be calculated by:

$$Am = x \times A \text{ down } a + y \times A \text{ down } b + z \times A \text{ down } c \quad (7)$$

$$x^2 + y^2 + z^2 = (2r)^2 \quad (8),$$

where "x", "y", and "z" are the Cartesian coordinates for the path length of the light ray constrained to lie on a sphere of radius "r". These coordinates can be converted to spherical coordinates as well:

$$x = 2r \times \sin\theta \times \cos\varphi \quad (9)$$

$$y = 2r \times \sin\theta \times \sin\varphi \quad (10)$$

$$z = 2r \times \cos\theta \quad (11),$$

where θ is the inclination from the z axis and φ is the inclination from the x axis (**Figure 6**).

The predicted colors under CIE D65 and CIE A illuminants (daylight equivalent and incandescent illuminants) for the alexandrite cuboid in this study are mapped out in **Figure 7** for any direction through an alexandrite wafer with path lengths of 1, 5, 10, and 20 mm (see appendix 1 for color maps with path length of 15 and 25mm).

The color maps in **Figure 7** show that under CIE D65 illumination (daylight equivalent) the calculated color of the alexandrite, overall, is mostly slightly bluish-green except when light passes nearly along the b-axis where it takes on more of a brownish-yellow to brownish-pink or brownish-red hue. This brownish region grows as the light path length is increased until 20 mm where it begins to dominate the D65 color map at a much wider range of orientations (i.e., a larger portion of the map). This is a manifestation of the "Usambara effect" wherein the hue and color of a mineral change as path length increases. This is due to the fact that the Cr^{3+} absorptions create two transmission windows in the red and blue/green portions of the visible spectrum (**Figures 2-3**), and as the path length increases, one of these windows is preferentially "closed" relative to the other. In this case, when the material gets thicker the transmission in the blue/green window decreases faster than in the red window causing the stone to become more red in more orientations.

Under CIE A illumination (incandescent light) the calculated color for the alexandrite is overall pink to red when light travels nearly along the b-axis and violet to blue with light traveling nearly perpendicular to the b-axis (i.e. traveling along the a- or c-axis or in between them). Again, as path length increases, the reddish region becomes dominant at a wider range of

orientations due to the "Usambara effect". With both D65 and A illumination the calculated color gets darker (decreasing L* coordinate) and the chroma increases (increasing C_{ab}* coordinate) as the light path length increases.

Chroma maps

The chroma maps under A and D65 illuminations are shown in **Figure 8** as well as the calculated chroma difference (chroma describes the saturation of the color). Unsurprisingly, with a path length of 1mm the chroma is low under both lighting conditions. As path length is increased, values of chroma become larger, especially for light passing along the a or b crystallographic axes for A illumination and in a range of orientations for light passing between the a- and c-axes under D65 illumination.

Optimal color change is usually produced when there is little difference between the chroma values under A and D65 illuminations. This is due to the fact that when the chroma difference is large, it can be caused by a low chroma value under one of the two illuminants. In this case the alexandrite under that illuminant will be an unattractive grayish or brownish color instead of a well-saturated blue-green or red. In general, a good color change occurs when the chroma difference is small.

Under incandescent illumination A, light passing along the c-axis will have low values of chroma except at longer path lengths. The same is true for light passing along the b-axis under daylight-equivalent illumination D65. The chroma difference is relatively large for light passing along the b- and c-axes, but these orientations will produce a less valuable color change for smaller stones as the color under daylight or incandescent light will be less saturated. Additionally, at longer path lengths (>15 mm) values of chroma decrease significantly in most

orientations under daylight-equivalent D65 lighting (except along the a, b, and c crystallographic axes).

From the color maps in **Figure 7** it is obvious that the calculated colors for the alexandrite become darker at 20 mm. This is due to a decrease in the lightness of the stone (L*). At 5 mm path length there is a large chroma difference between the two illuminants near the c-axis (**Figure 8**). At longer path lengths the chroma difference for light passing nearly along the b-axis begins to grow and dominate the chroma difference maps.

Hue angle difference maps

Areas with large values of hue angle difference do not necessarily show a good color change. If one or both of the hues have very low chroma, the hue will simply be a brownish or grayish color. In the hue angle difference maps for the calculated color for a path length of 1mm to 5mm, a critical point appears near the c axis at 1mm path length (**Figure 9**). The upper side of the critical point shows a very low hue angle difference and lower side shows a very high hue angle difference at 1 mm path length. This anomalous critical point occurs because the calculated chroma is very low in this region under A illumination and the calculated colors all plot very near the origin of the a*-b* field. Therefore, as the calculated color shifts from one side of the origin to another the hue angle changes dramatically creating this critical point in the hue angle difference plot. Nonetheless, the calculated colors in this region vary smoothly and appear very similar (**Figure 7**). The critical point disappears when path length increases and the chroma increases pushing the calculated colors away from the a*-b* origin. At 5 mm path length, the highest hue angle difference region starts from the edge between the a and b crystallographic axes and extends to the upper portion of the edge between the b and c axes (**Figure 9**). The area

near the a axis shows a relatively low hue angle difference from 1 to 5mm path length (**Figure 9**).

For a 10 mm path length, the highest hue angle region becomes smaller and moves to an area that starts from the upper center of the edge between the b and c axes and extends to the center of the a, b and c axes. A critical point appears in this plot as well. The upper side shows a very high hue angle difference and the lower side shows a very low hue angle difference. The critical point forms because the hue angle under D65 illumination changes significantly around the critical point area. However, the calculated colors at 10 mm for D65 illumination vary smoothly and appear very similar in this region (**Figure 7**). Again, as for the 1 and 5 mm path lengths above, this critical point occurs because the chroma is low in this region.

At 20 mm path length (**Figure 9**), the critical point moves close to the center of the edge between b and c axes. The large area near b axis shows the lowest hue angle difference here (**Figure 9**).

Color difference maps

From maps in **Figure 10** we notice that the color difference increases first when the path length increases from 1 to 10 mm, and starts to decrease from 10 to 20 mm path length. Most importantly, these maps show generally that the strongest absolute color difference occurs not when light passes along one of the three crystallographic axes, but in an orientation somewhere between these three axes. In fact, except at very long light path lengths (i.e. 20 mm), the absolute color difference is generally smaller along the crystallographic axes than at some intermediate orientation. This is especially true for light passing along the b-axis which always has the lowest color difference between A illumination and D65 illumination. However, it can be seen in

Figure 10 that the area of maximum color difference does shift from approximately equally among the three axes at 1 mm toward the a- and c-axes join from 5 to 10 mm and toward the c-axis at 20 mm.

It should be stressed, however, that the absolute color difference is not necessarily going to be the most attractive or desirable color change phenomenon possible. The classic "Alexandrite effect" was used to describe Cr-bearing chrysoberyl which exhibited a blue to green color in daylight and a red to purple color in incandescent light. Therefore, even if a certain orientation gives a larger absolute color difference the resulting color change phenomenon may be less desirable than an orientation with a smaller absolute color difference but with red and green hues associated with the classical "Alexandrite effect".

For this reason we define a region for "optimal color change" wherein the hue angle calculated for A illumination must be in the range between 0˚ to 30˚, or 330˚ to 360˚ (the red-purple region in $L^*c_{ab}^*h_{ab}^*$ space**, Figure 11**) and the hue angle calculated for D65 illumination must be in the range of 135˚ to 285˚ (green-blue region in $L^*c_{ab}^*h_{ab}^*$ space, **Figure 11**). Additionally, we specify that the chroma value for both calculated colors must be larger than 5. We will consider our alexandrite with a calculated 10 mm light path length and plot this "optimal color change" region on the color map showing the "optimal" orientation (**Figure 12**). Furthermore, we can define an "unfavorable color change" region in which the hue angles calculated for our alexandrite under A and D65 illumination both lie within the green-blue region of the $L^*c_{ab}^*h_{ab}^*$ space from 135˚ to 285˚ or that they both lie within the red-purple region from 0˚ to 30˚, or 330˚ to 360˚ (**Figure 11**). This "unfavorable color change" region is also plotted in **Figure 12**. The "optimal" range lies in a narrow strip near the b-axis stretching between the a- and c-axes. The "unfavorable" region lies in a swath stretching between the a- and c-axes. Note

that this "unfavorable" region actually coincides with the area with the largest absolute color difference from **Figure 10**. However, in this region the color changes from bluish-green in D65 illumination to violetish-blue in A illumination. This is in opposition to the more classical shift from purplish-red to green under incandescent and daylight conditions as seen for the "optimal" region in **Figure 12**.

To decide on a single "best" color change orientation with 10 mm path length for this material, we select the spot with highest color difference in the optimal color change region. The "best" color change orientation spot is marked in **Figure 12** as a red circle. The Cartesian coordinate and spherical coordinate systems for this orientation are:

$$x \text{ (a-axis)} = 0.1267,\ y \text{ (b-axis)} = 3.1441,\ z \text{ (c-axis)} = 3.8857,$$

$$\theta = 39.00°,\ \varphi = 87.69°,\ r = 5 \text{ mm}$$

With θ being the inclination from the c axis and φ being the inclination from the a axis. The color difference here is 30.86, the hue angle difference is 159.11°, and the chroma difference is 4.69.

Calculating color and color change for a faceted stone

In a faceted stone the color behavior is very different from what is observed in a wafer. This is because light that passes through the table of a well-cut stone (i.e. the top of the stone) will be reflected off one of the bottom pavilion facets toward an opposing pavilion facet before it is reflected back up through the table. When the light is passing from pavilion to pavilion facet, it travels in a different direction than when it entered the stone and so the absorption of that light ray through the stone is a mixture of different orientations. For instance, if the table is oriented perpendicular to the c-axis, the absorption for a light ray that enters the stone, bounces off the

412 pavilion facets, and exits through the table again will be a mixture of absorptions of light down
413 the c-axis plus absorption down the a- and/or b-axes (**Figure 13**). Hughes, et al., (2014)
414 illustrated the simplified face-up appearance of a biaxial faceted stone without considering the
415 possibility of an "Alexandrite affect". In their model, a faceted biaxial stone can be separated
416 into three areas, which are D, E and F corresponding to the colors observed in the inner, middle,
417 and outer regions for a face-up faceted stone. The color seen for region D will be similar to that
418 seen for a wafer. However, light that enters the stone in regions E and F will take a path
419 involving internal reflection from one side of the pavilion (bottom of the faceted stone) to the
420 other side and then refraction again to take the light back out through the top of the stone to the
421 observer. When the light bounces between opposite ends of the pavilion the optical absorption
422 will be different than if the light simply passed through the stone completely in the original
423 orientation. In other words, regions E and F will have their colors altered by mixing with light
424 traveling in orientations different from the initial light pathway

425 A schematic map with fifteen spots evenly distributed between three crystallographic
426 axes is shown in **Figure 14** to provide a direct comparison of the color pairs of the inner region
427 of a faceted stone (area D, **Figure 13**) under D65 and A illumination. The color pairs in this map
428 correspond also to the colors expected for a wafer oriented in any of these directions. Note that
429 the color difference (ΔE^*ab) is nearly the same for circled color pairs 1 and 2 in **Figure 14**.
430 However, color pair 2 shows the classical shift between red and green while color pair 1 shifts
431 between bluish-purple and bluish-green. The color change for color pair 2 would generally be
432 considered to be more desirable.

433 Suppose the table of our hypothetical stone is cut perpendicular to the c axis. To a first
434 approximation, we assume that the pavilion-to-pavilion path length is 1/3 of the total path length

435 through the stone for region E (**Figure 13**). Then, assuming equal mixing of absorption along the
436 a- and b-axes when light passes from pavilion-to-pavilion, the absorption of light being reflected
437 through the middle region of the stone (region E, **Figure 13**) can be calculated as:

438 $$\text{Ae down c} = \frac{4}{6}\times\text{A down c} + \frac{1}{6}\times\text{A down b} + \frac{1}{6}\times\text{A down a} \quad (11)$$

439 When the table is oriented along the a- and/or b-axes the absorption for the middle region (E,
440 **Figure 13**) can be calculated as:

441 $$\text{Ae down a} = \frac{4}{6}\times\text{A down a} + \frac{1}{6}\times\text{A down b} + \frac{1}{6}\times\text{A down c} \quad (12)$$

442 $$\text{Ae down b} = \frac{4}{6}\times\text{A down b} + \frac{1}{6}\times\text{A down a} + \frac{1}{6}\times\text{A down c} \quad (13)$$

443

444 Now for the outer rim of the faceted stone, we assume that the path length is dominantly
445 composed of the pavilion-to-pavilion path. Then we can roughly calculate the absorption of a
446 light ray passing through a stone oriented with the table perpendicular to the a-, b-, or c-axes as:

447 $$\text{Af down a} = \frac{1}{2}\times\text{A down b} + \frac{1}{2}\times\text{A down c} \quad (14)$$

448 $$\text{Af down b} = \frac{1}{2}\times\text{A down a} + \frac{1}{2}\times\text{A down c} \quad (15)$$

449 $$\text{Af down c} = \frac{1}{2}\times\text{A down a} + \frac{1}{2}\times\text{A down b} \quad (16)$$

450 Now we can plot calculated colors under A and D65 illumination for a faceted stone with
451 10 mm path length in each of these regions (D, E, and F, **Figure 13**). We can further combine
452 these three regions into the inner, middle, and outer regions of a single color circle and plot the

453 results under A and D65 illumination for a variety of orientations (**Figure 15**). These mixed
454 color circles give us some sense of what a faceted alexandrite would look like when oriented at
455 various intervals between the three crystallographic axes (**Figure 15**). Similar to our analysis
456 from above, the area close to c axis is not an optimal area because of the low chroma under A
457 illumination which presents itself as a grayish contribution to these color circles. Orienting the
458 table facet closer to a and b axis is also not optimal because there is always an area (inner,
459 middle or outer) of stone showing an unfavorable pair of hues (i.e. low hue angle difference).
460 The designation of the "best" color change area is inherently subjective. However, the region
461 lying about 30° off the b-axis approximately midway between the a- and c-axes appears to show
462 the strongest shift between reddish-purple and bluish-green hues which are characteristic of the
463 classical Alexandrite effect. Nonetheless, these color maps show that when pleochroism is
464 considered for a faceted gemstone, the requirements for "optimal" orientation are relaxed
465 significantly and there are a wide range of orientations that can produce a stone showing color
466 change from red-purple to green-blue between incandescent and daylight illumination,
467 respectively.

468 **Implications**

469 The current contribution demonstrates the intricacies of the color change (or alexandrite)
470 effect in a mineral that also displays pleochroism. While there are certainly orientations of this
471 sample that show weak color change and are therefore less desirable, there is no single "best"
472 direction for the material but a broad range of acceptable orientations. The situation for a facetted
473 gemstone fashioned out of this material is even more complicated as light passes through this
474 pleochroic crystal in multiple directions. Hence, the colors of the light rays returning to the eye
475 are the product of a mixture of the absorption spectra from various crystallographic directions.

Using a simple model to account for this problem, we find that pleochroism in a facetted gemstone serves to smear out the "best" direction for color change. The calculations here suggest that for a reasonably sized stone using this specific material, the requirements for orientation for the finished gemstone are relatively loose as long as a certain relatively narrow range of orientations is avoided. As stated from the outset, color has long been one of the major tools mineralogists employ in their day to day work. Color is used not only to identify minerals but also to identify potential treatments to gems, chemical signatures, and sometimes to unravel a minerals geological history. However, as we have shown here, in many cases, the color observed in a mineral or gem is a complicated interplay between not only chromophore concentration but also light path length, orientation in non-cubic stones, and the specific lighting conditions used. The techniques outlined here can be used as guidelines for future studies of the intracacies in color science as it applies to the worlds of mineralogy and gemology.

Acknowledgments

The authors thank Elise Skalwold for her thorough review as well as the associate editor Aaron Celestian for handling the manuscript. Many thanks are also owed to Chi Ma of Caltech for his assistance with EPMA measurements. The authors thank James Shigley from Gemological Institute of America for his constructive comments. We thank Mike Breeding, Dino DeGhionno, Shane McClure, Nathan Renfro, David Nelson, Troy Ardon, and Tao Hsu from Gemological Institute of America and David Patterson from the Geminex Corporation for many helpful mineralogical and colorimetric discussions. This study was supported by Gem Identification Department in Gemological Institute of America, Carlsbad, United States.

References cited

Anderson, B.W. (1950) Gemstones and the spectroscope - the absorption spectra of emerald and alexandrite. Gems & Gemology, 6, 263-266.

Bamford, C.R. (1977) Colour generation and control in glass. Glass Science and Technology 2, 71 p. Elsevier Scientific Publishing Company, Amsterdam-Oxford-New York.

Bosi, F., Andreozzi, G.B., Halenius, U., and Skogby, H. (2015) Experimental evidence for partial Fe^{2+} disorder at the Y and Z sites of tourmaline: A combined EMP, SREF, MS, IR and OAS study of schorl. Mineralogical Magazine, 79, 515-528.

Bragg, W. L., and Brown, G. B. (1926) The crystalline structure of chrysoberyl. Proceedings of the Royal Society of London, Series A, Containing Papers of a Mathematical and Physical Character, 110, 34-63.

Bukin, G.V., Matrosov, V.N., Orekhova, V.P., Remigailo, Y.L., Sevastyanov, B.K., Syomin, E.G., Solntsev, V.P., and Tsvetkov, E.G. (1981) Growth of alexandrite crystals and investigation of their properties. Journal of Crystal Growth, 102, 1037-1041.

CIE Commission Internationale de I'Éclairage (1931) Proceedings of the 8th Session of CIE, 19-29 p. Cambridge, England.

CIE Commission Internationale de I'Éclairage (1977) CIE Recommendations on Uniform Color Space, Color-Difference Equations, and Metric Color Terms. Color Research & Application, 2, 5-48.

CIE Commission Internationale de I'Éclairage (2004) CIE 110: Technical Report: Colorimetry. 3rd edition.

518 Bloss, F. (1961) An introduction of the methods of optical crystallography. Holt, Rinehart, and
519 Winston, New York. pp. 294.

520 Collins, A.T. (1980) Colour centres in diamond. Journal of Gemmology, 18, 37-75.

521 Dudka, A. P., Sevastyanov, B. K., and Simonov, V. I. (1985) Refinement of atomic structure of
522 alexandrite. Soviet Physics - Crystallography, 30, 277-279.

523 Erukhimovitch, V., Mordekoviz, Y., and Hayun, S. (2015) Spectroscopic study of ordering in
524 non-stoichiometric magnesium aluminate spinel. American Mineralogist, 100, 1744-1751.

525 Farrell, E. F., and Newnham, R. E. (1965) Crystal-field spectra of chrysoberyl alexandrite,
526 peridot, and sinhalite. American Mineralogist, 50, 1972-1981.

527 Farrell, E. F., Newnham, R. E., and Fang, J.H. (1963) Refinement of chrysoberyl structure.
528 American Mineralogist, 48, 804.

529 Fregola, R.A., Skogby, H., Bosi, F., D'Ippolito, V., Andreozzi, G.B., and Halenius, U. (2014)
530 Optical absorption spectroscopy study of the causes for color variations in natural Fe-bearing
531 gahnite: Insights from iron valency and site distribution data. American Mineralogist, 99, 2187-
532 2195.

533 Garcia-Lastra, J. M., Aramburu, J. A., Barriuso, M.T., and Moreno, M. (2006) Optical properties
534 of Cr^{3+}-doped oxides: Different behaviour of two centers in alexandrite. Physical Review B, 74,
535 115-118.

536 Geiger, C.A., Stahl, A., and Rossman, G.R. (2000) Single-crystal IR- and UV/VIS-spectroscopic
537 measurements on transition-metal-bearing pyrope. European Journal of Mineralogy, 2000, 259-
538 271.

539 Gübelin, E. J., and Schmetzer, K. (1980) The alexandrite effect in minerals: Chrysoberyl, garnet,
540 corundum, fluorite. Neues Jahrbuch für Mineralogie Abhandlungen, 138, 147-164.

541 Gübelin, E. J., and Schmetzer, K. (1982) Gemstones with Alexandrite Effect. Gems &
542 Gemology, 18, 197-203.

543 Guo, X.A., Zhang, B.X., Wu, L.S., and Chen, M.L. (1986) Czochralski growth and laser
544 performance of alexandrite crystals. American Institute of Physics - Conference Proceedings,
545 146, 249-250.

546 Guo, X.G., Chen, M.L., Li, N.R., Qin, Q.H., Huang, M.F., Fei, J.W., Wen, S.L., Li, Z.Q. and
547 Qin, Y. (1987) Czochralski growth of alexandrite crystals and investigation of their defects.
548 Journal of Crystal Growth, 83, 311-318.

549 Halvorsen, A., and Jensen, B. B. (1997) A new color change effect. Journal of Gemmology, 210,
550 3210–3230.

551 Halvorsen, A. (2006) The Usambara effect and its interaction with other color change
552 phenomena. Journal of Gemmology, 30, 1–21.

553 Hassan, F., and El-Rakhawy, A. (1974) Chromium III centers in synthetic alexandrite. American
554 Mineralogist, 59, 159-165.

555 Howell, D., Fisher, D., Piazolo, S., Griffin, W.I., and Sibley, S.J. (2015) Pink color in Type I
556 diamonds: Is deformation twinning the cause? American Mineralogist, 100, 1518-1527.

557 Hughes, R. W. (2014) Pleochroism in faceted gems: an introduction. Gems & Gemology, 100,
558 216-226.

559 Hurlbut Jr, C. S. (1971) Dana's Manual of Mineralogy, John Wiley and Sons Inc., New York.

560 Kozak, P.K., Duke, E.F., and Roselle, G.T. (2004) Mineral distribution in contact-
561 metamorphosed siliceous dolomite at Ubehebe Peak, California, based on airborne imaging
562 spectrometer data. American Mineralogist, 89, 701-713.

563 Krambrock, K., Pinheiro, M.V.B., Guedes, K.J., Medeiros, S.M., Schweizer, S., Spaeth, J.-M.
564 (2004) Correlation of irradiation-induced yellow color with the O^- hole center in tourmaline.
565 Physics and Chemistry of Minerals, 31, 168-175.

566 Ling, Z.C., Wang, A., Jollif, B.L., Arvidson, R.E., and Xia, H.R. (2008) A systematic Raman,
567 mid-IR, and Vis-NIR spectroscopic study of ferric sulfates and implications for sulfates on Mars.
568 39^{th} Lunar and Planetary Science Conference, p. 1463.

569 Liu, Y., Shigley, J. E., Fritsch, E., and Hemphill, S. (1994) The "alexandrite effect" in
570 gemstones. Color Research and Application, 19, 186–191.

571 Liu, Y., Shigley, J. E., Fritsch, E., and Hemphill, S. (1995a) Abnormal Hue-Angle change of the
572 gemstone tanzanite between CIE illuminants D65 and A in CIELAB color space. Color Research
573 and Application, 20, 245-250.
574 Liu, Y., Shigley, J. E., Fritsch, E., and Hemphill, S. (1995b) Relationship between the
575 crystallographic origin and the "alexandrite effect" in synthetic alexandrite. Mineralogical
576 Magazine, 59, 111-114.
577 Liu, Y., Shigley, J. E., Fritsch, E., and Hemphill, S. (1999a) A colorimetric study of the
578 alexandrite effect in gemstones. Journal of Gemmology, 26, 371–3810.

579 Nassau, K., (1983) The Physics and Chemistry of Color: The Fifteen Causes of Color, John
580 Wiley & Sons, New York.

581 Pearson, G. M., and Hoover, D. B. (2013) Dichromatism, the cause of the Usambara and the
582 alexandrite colour-change effects. Australian Gemmologist, 25, 62-70.

583 Powell, R. C., Xi, L., Gang, X., Quarles, G.J., and Walling, J.C. (1985) Spectroscopic properties
584 of alexandrite crystals. Physical Review B, 32, 2788-2797.

585 Reinitz, I.M. and Rossman, G.R. (1988) Role of natural radiation in tourmaline coloration.
586 American Mineralogist, 73, 822-825.

587 Rossman, G.R. (2014) Optical spectroscopy. Reviews in Mineralogy and Geochemistry, 78, 371-
588 398.

589 Schmetzer, K., (2012) Natural alexandrites and chrysoberyls from Madagascar with irregular and
590 regular growth patterns. Australian Gemmologist, 24, 243-248.

591 Schmetzer, K., and Bosshart, G. (2010) Colorimetric data of Russian alexandrite and yellowish
592 green to green chrysoberyl. In: Schmetzer, K. Russian alexandrites, pp. 107-120. Schweizerbart
593 Science Publishers, Stuttgart.

594 Schmetzer, K., and Malsy, A. K. (2011) Alexandrite and colour-change chrysoberyl from the
595 Lake Manyara alexandrite-emerald deposit in northern Tanzania. Journal of Gemmology, 32,
596 179-209.

597 Schmetzer, K., Bernhardt, H. J., Bosshart, G., and Hainschwang, T. (2009) Color-change garnets
598 from Madagascar: variation of chemical, spectroscopic and colorimetric properties. Journal of
599 Gemmology, 31, 2310–282.

600 Schmetzer, K., Bernhardt, H. J., and Hainschwang, T. (2012) Flux-grown synthetic alexandrites
601 from Creative Crystals. Journal of Gemmology, 33, 49-81.

602 Schmetzer, K., Bernhardt, H. J., Balmer, W. A., and Hainschwang, T. (2013) Synthetic
603 alexandrites grown by the HOC method in Russia: internal features related to the growth
604 technique and colorimetric investigation. Journal of Gemmology, 33, 113-129.

605 Smith, E.M., Helmstaedt, H.H., and Flemming, R.L. (2010) Survival of the brown color in
606 diamond during storage in the subcontinental lithospheric mantle. The Canadian Mineralogist,
607 48, 571-582.

608 Sobron, P., Bishop, J.L., Blake, D.F., Chen, B., and Rull, F. (2014) Natural Fe-bearing oxides
609 and sulfates from the Rio Tinto Mars analog site: Critical assessment of VNIR spectroscopy,
610 laser Raman spectroscopy, and XRD as mineral identification tools. American Mineralogist, 99,
611 1199-1205.

612 Sun, Z., Palke, A. C., and Renfro, N. (2015) Vanadium and chromium bearing pink pyrope
613 garnet: characterization and quantitative colorimetric analysis. Gems & Gemology, 51(4), 348-
614 369.

615 Thomas, T., Rossman, G. R., and Sandstrom, M. (2014) Device and method of optically
616 orienting biaxial crystals for sample preparation. Review of Scientific Instruments, 85, 093105.

617 Troup, G. J. (1969) The alexandrite effect. Australian Gemmologist, 10, 9-12.

618 Turner, D.J., Rivard, B., and Groat, L.A. (2016) Visible and short-wave infrared reflectance
619 spectroscopy of REE phosphate minerals. American Mineralogist, 101, 2262-2278.

White, W. B., Roy, R., and Critchton, J. M. (1967) The "alexandrite effect": An optical study. American Mineralogist, 52, 867-871.

Figure captions

Figure 1: The image on the left shows a schematic morphology of an un-twinned chrysoberyl crystal. The image on the right shows the three, mutually perpendicular, principal vibration axes, X, Y and Z. The unpolarized ray R1, parallel to Z axis, splits into two rays E||a and E||c when passing through the crystal. Similarly, R2 splits into E||b and E||c and R3 splits into two rays E||a and E||b.

Figure 2: The three polarized-light UV-Vis-NIR absorption spectra, E||a, E||b and E||c shown in blue, red, and green, respectively. Path length is normalized to 1 mm. Two transmission windows are seen in all spectra and are marked as A and B.

Figure 3: The three unpolarized-light UV-Vis-NIR absorption spectra for light traveling down the a-, b-, and c- axes corresponding to “A down a”, “A down b”, and “A down c”, respectively. “A down a”, “A down b”, and “A down c” are shown as purple, orange, and light blue, respectively. Path length is normalized to 1 mm. Path length is normalized to 1 mm. Two transmission windows are seen in all spectra and are marked as A and B.

Figure 4: Comparison between color observed in photographs of the rectangular cuboid along a, b and c axes (row 1) and the calculated color panels (row 2).

Figure 5: Graphs of three CIE1976 color circles with L* (lightness) = 25, 50 and 75 respectively. The maximum chroma value of the largest middle circle is 50 (C_{ab}* = 50). The maximum chroma value of two small circles is 29 (C_{ab}* = 29). L* (lightness, or the perceived

641 brightness or darkness) is defined vertically. C_{ab}*(chroma, or the saturation of a hue) is defined
642 radially and measured from center of each slice. The range of C_{ab}* is restricted at low and high
643 values of L* because at high (low) values of L*, the color becomes dominantly white (black) and
644 it is not possible to perceive a high saturation for other hues (or a high value of C_{ab}*).

645 **Figure 6:** The image on the left shows the color maps and colorimetric parameter maps of an
646 alexandrite wafer generated by calculating the spectra of unpolarized light in specific
647 orientations between a, b and c crystallographic axes. The image on the right shows the spherical
648 coordinate system used in this article as shown. Angle θ is inclination from the z axis direction
649 and azimuthal angle φ is measured from Cartesian x axis (y axis has φ = +90˚, x = a axis, y = b
650 axis, z = c axis).

651 **Figure 7:** Calculated color maps of an alexandrite wafer between the three crystallographic axes
652 with path length 1 mm, 5 mm, 10 mm and 20 mm. The left column of the color maps are under
653 CIE D65 illumination (i.e. daylight), while and right column of the color maps are under CIE A
654 illumination (i.e. incandescent). The color maps with path lengths of 15 and 25 mm are included
655 as supplemental figures in the data depository.

656 **Figure 8:** Chroma (C^*_{ab}) maps under CIE A illumination (incandescent light, left column), CIE
657 D65 illumination (daylight, middle column), and the difference map (right column). Path lengths
658 were normalized to 1mm, 5mm, 10mm and 20mm. Additional maps of chroma at various path
659 lengths as well as animations are included as supplemental figures in the data depository.

660 **Figure 9:** Maps of the hue angle difference (Δh^*_{ab}) between CIE A and D65 illumination
661 (incandescent and daylight illumination, respectively). Path lengths are normalized to 1mm,

5mm, 10mm and 20mm. Maps for additional path lengths from 1mm to 25mm and animations are included as supplemental figures in the data depository.

Figure 10: Maps of the color difference (ΔE^*_{ab}) between CIE A and D65 illumination (incandescent and daylight illumination, respectively). Path lengths are normalized to 1mm, 5mm, 10mm and 20mm. The completed maps from 1mm to 25mm are attached in the Appendix 1 (Section 2, Figure 6, page 6). Maps for additional path lengths from 1mm to 25mm and animations are included as supplemental figures in the data depository.

Figure 11: The CIELAB 1976 Color Circle showing the green-blue region with values of h^*_{ab} between 135˚ to 285˚ and the red-purple region with h^*_{ab} between 0˚ to 30˚ and 330˚ to 360˚.

Figure 12: "Optimal" and "unfavorable" orientations for an alexandrite wafer with 10 mm path length. The color maps show the colors that would be seen in either region under daylight-equivalent illumination (D65) or incandescent illumination (A).

Figure 13: Schematic diagrams of light pathways through the hypothetical faceted gemstone considered here. Pleochroic colors will be seen in the face up gemstone due to mixing of light travelling in different directions through the stone. For our purposes the gemstone is divided into inner, middle, and rim regions (modified after Hughes et al., 2014).

Figure 14: Fifteen color pairs for the alexandrite calculated for a 10 mm wafer in different crystallographic orientations. For each color pair, the left color is calculated for CIE A illumination (incandescent light) while the right color panel is for CIE D65 illumination (daylight). The color difference value of the color pair 1 is nearly the same as color pair 2.

682 **Figure 15:** Fifteen color pairs for the alexandrite calculated for a hypothetical faceted gemstone
683 with a 10 mm light path length with the table oriented in various crystallographic directions. For
684 each color pair, the left color is calculated for CIE A illumination (incandescent light) while the
685 right color panel is for CIE D65 illumination (daylight).The color pairs have been divided into
686 the "best" and "unfavorable" orientations.

687 **Tables**

Table 1: EPMA and LA-ICP-MS data for four separate analyses of synthetic alexandrite

EPMA results - wt.%				*atoms per formula unit*[1]			*EPMA*	*LA-ICP-MS*
Al_2O_3	Cr_2O_3	BeO^2	wt.% total	Al	Cr	Be	Cr (ppmw)	Cr (ppmw)
76.58	0.21	18.82	95.61	1.996	0.004	1	1407	1291
77.02	0.20	18.93	96.14	1.997	0.003	1	1352	1378
76.63	0.20	18.83	95.66	1.996	0.004	1	1378	1368
77.05	0.19	18.93	96.17	1.997	0.003	1	1304	1435

1. Atoms per formula unit ($Be[Al,Cr]_2O_4$)
2. Calculated based on stoichiometric chrysoberyl formula

688

This is a preprint, the final version is subject to change, of the American Mineralogist (MSA)
Cite as Authors (Year) Title. American Mineralogist, in press.
(DOI will not work until issue is live.) DOI: http://dx.doi.org/10.2138/am-2017-6011

Figure 1

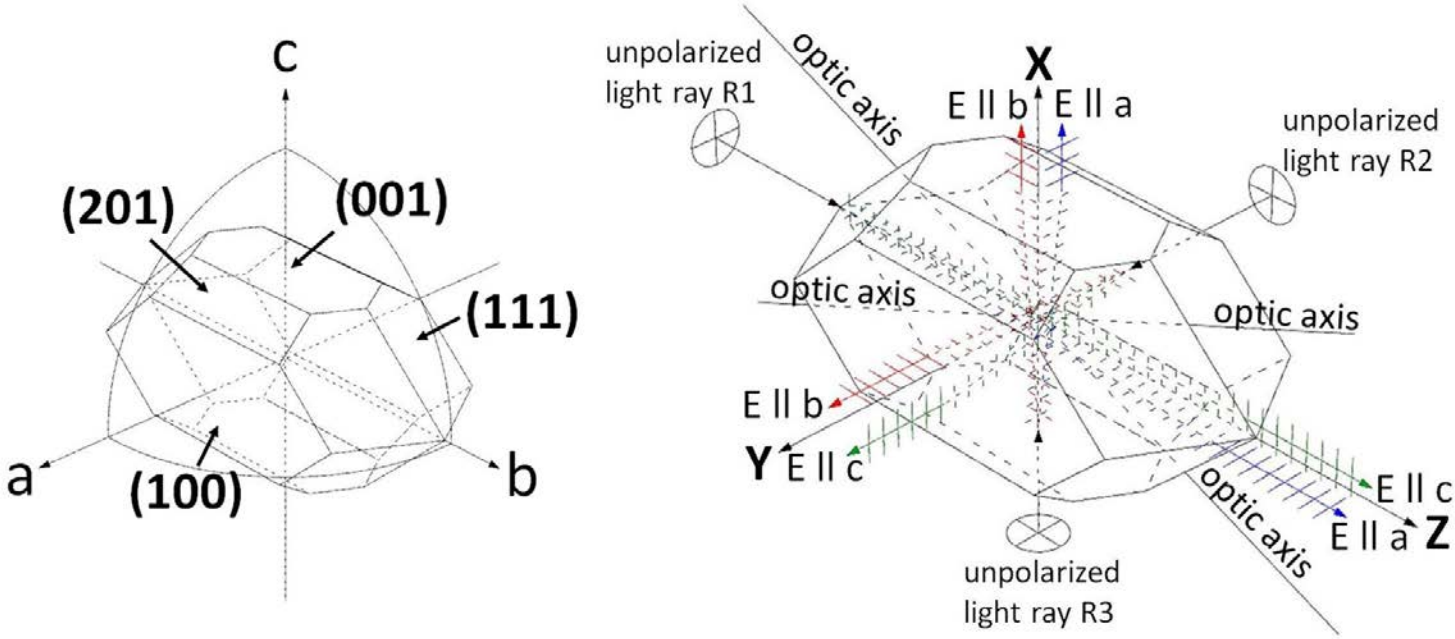

This is a preprint, the final version is subject to change, of the American Mineralogist (MSA)
Cite as Authors (Year) Title. American Mineralogist, in press.
(DOI will not work until issue is live.) DOI: http://dx.doi.org/10.2138/am-2017-6011

Figure 2

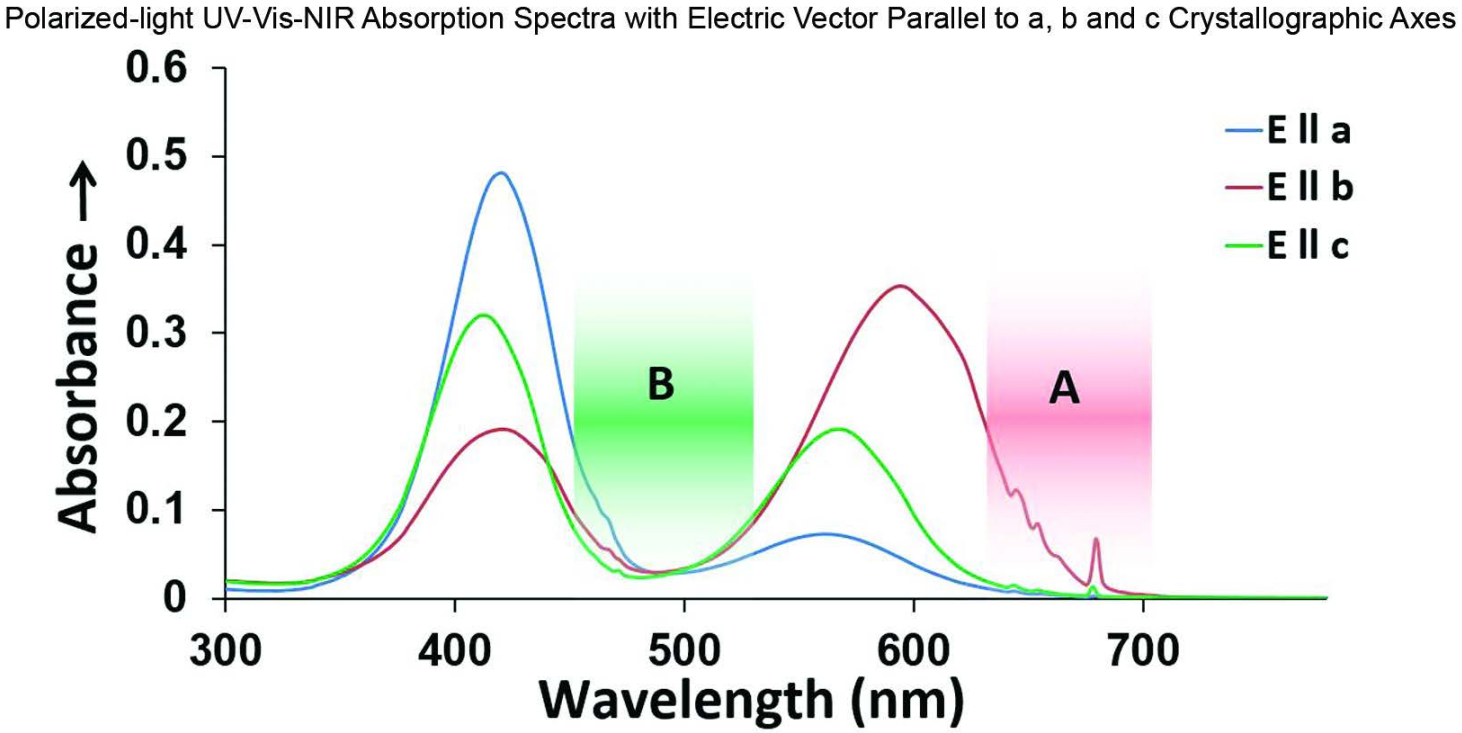

This is a preprint, the final version is subject to change, of the American Mineralogist (MSA)
Cite as Authors (Year) Title. American Mineralogist, in press.
(DOI will not work until issue is live.) DOI: http://dx.doi.org/10.2138/am-2017-6011

Figure 3

Unpolarized-light UV-Vis-NIR Absorption Spectra with Propagation Direction Parallel to a, b and c Crystallographic Axes

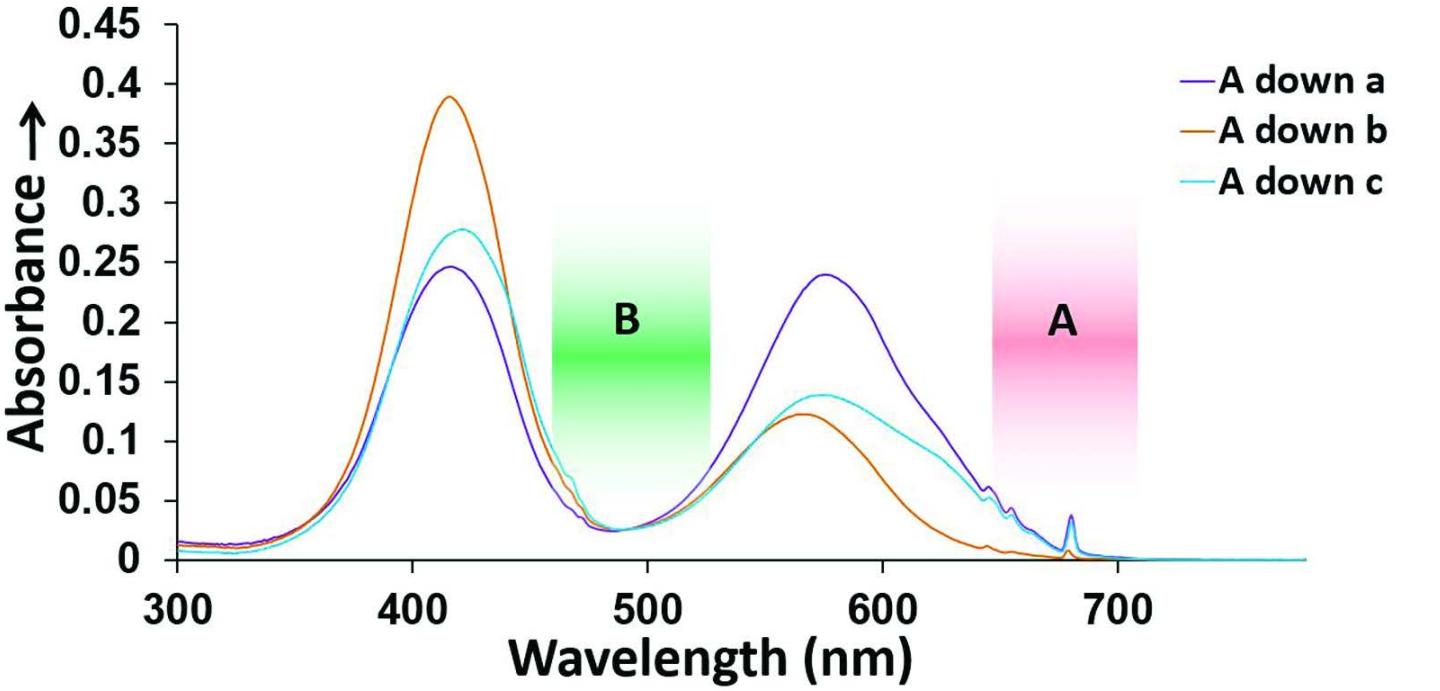

This is a preprint, the final version is subject to change, of the American Mineralogist (MSA)
Cite as Authors (Year) Title. American Mineralogist, in press.
(DOI will not work until issue is live.) DOI: http://dx.doi.org/10.2138/am-2017-6011

Figure 4

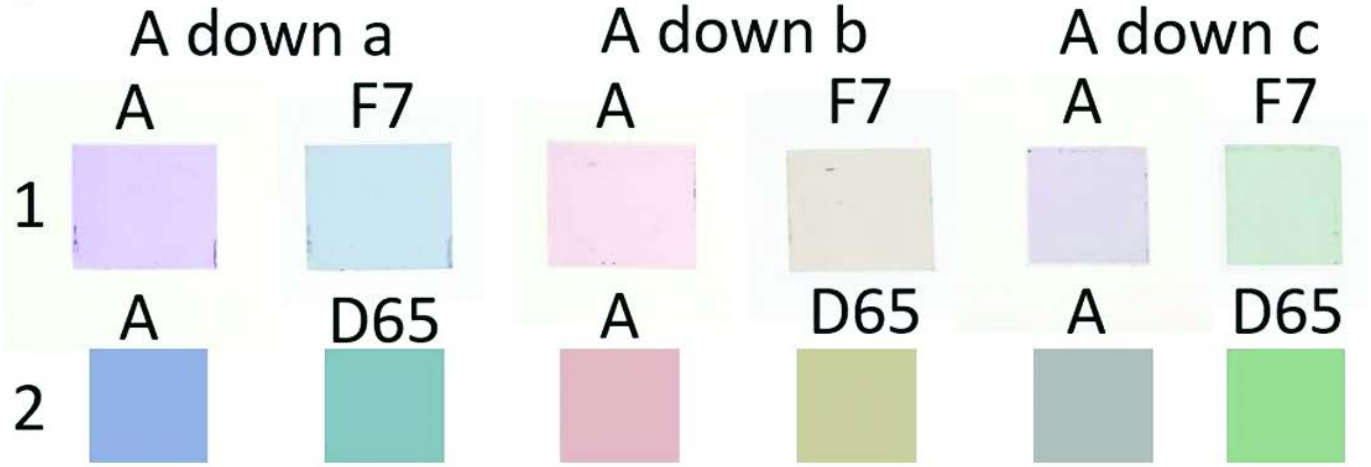

This is a preprint, the final version is subject to change, of the American Mineralogist (MSA)
Cite as Authors (Year) Title. American Mineralogist, in press.
(DOI will not work until issue is live.) DOI: http://dx.doi.org/10.2138/am-2017-6011

Figure 5

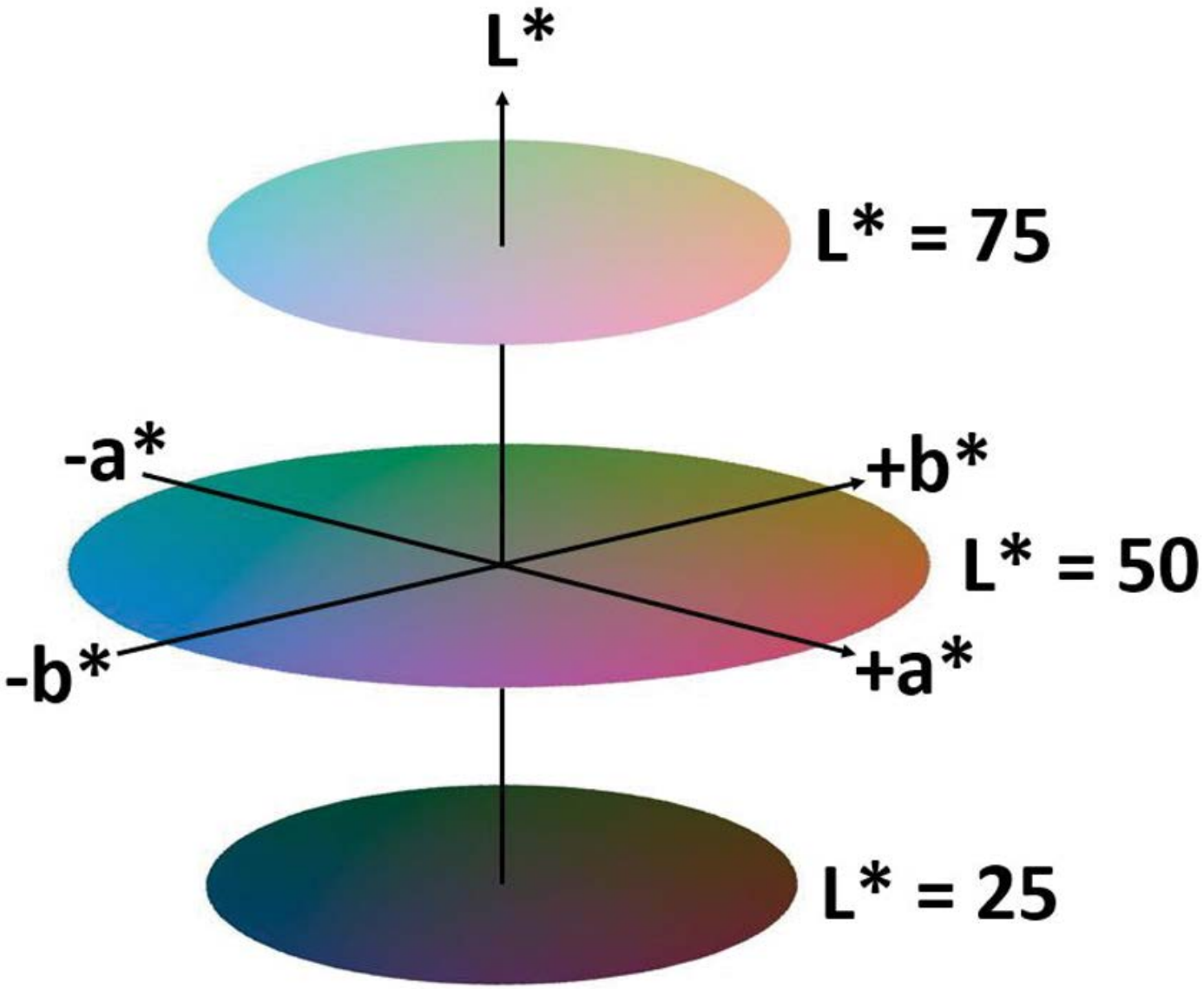

This is a preprint, the final version is subject to change, of the American Mineralogist (MSA)
Cite as Authors (Year) Title. American Mineralogist, in press.
(DOI will not work until issue is live.) DOI: http://dx.doi.org/10.2138/am-2017-6011

Figure 6

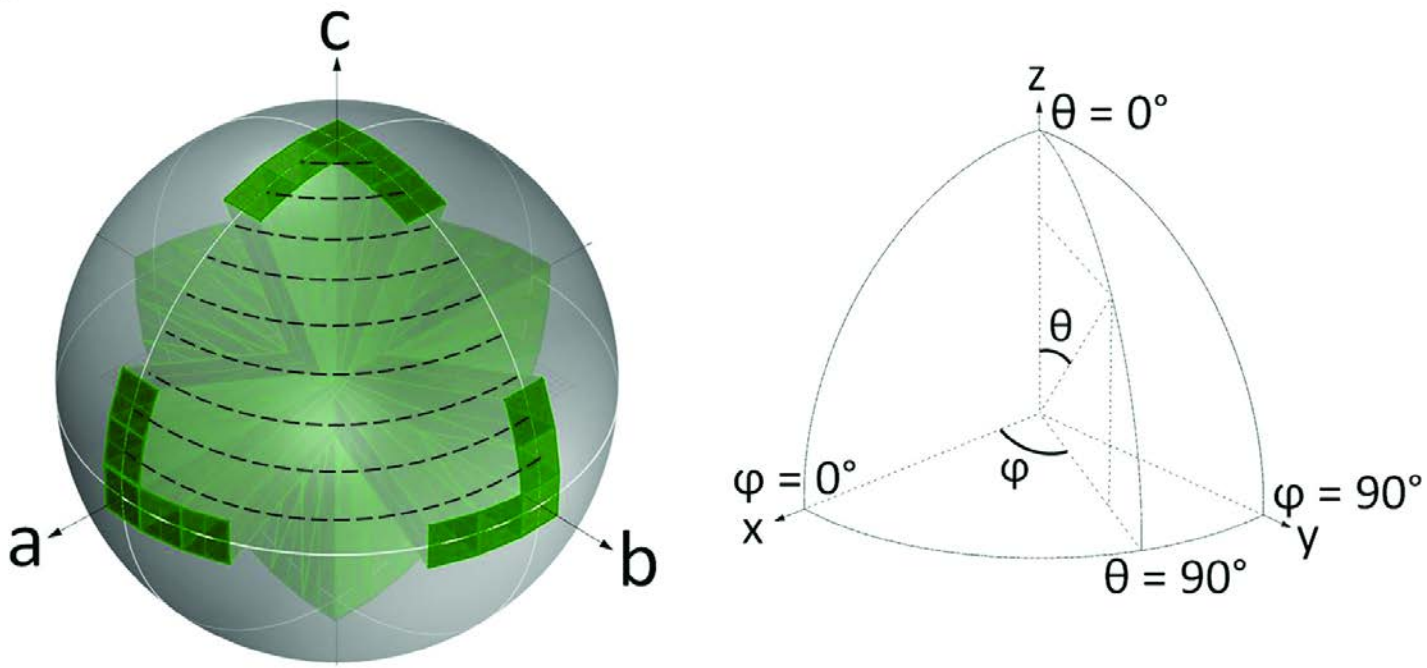

This is a preprint, the final version is subject to change, of the American Mineralogist (MSA)
Cite as Authors (Year) Title. American Mineralogist, in press.
(DOI will not work until issue is live.) DOI: http://dx.doi.org/10.2138/am-2017-6011

Figure 7

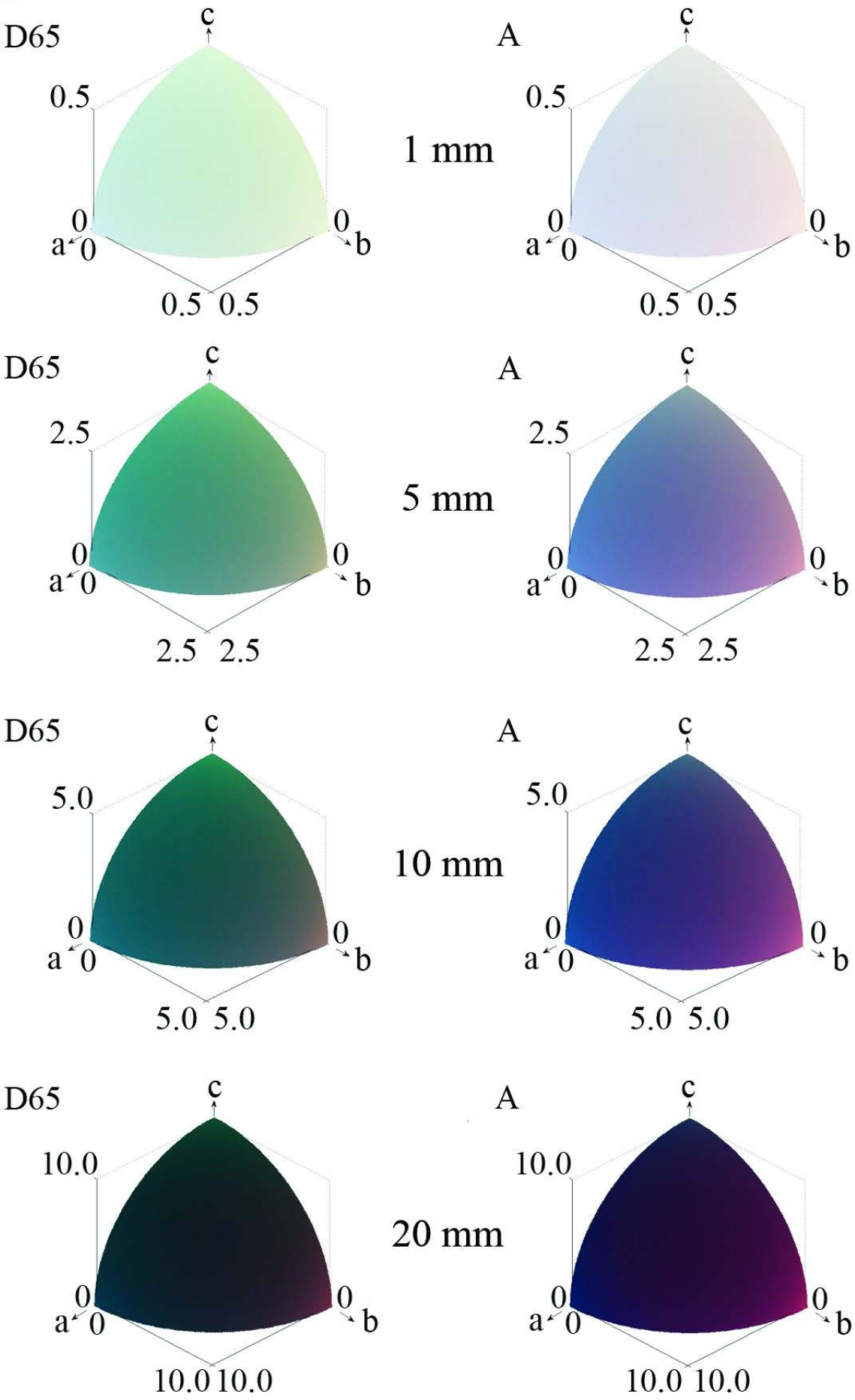

This is a preprint, the final version is subject to change, of the American Mineralogist (MSA)
Cite as Authors (Year) Title. American Mineralogist, in press.
(DOI will not work until issue is live.) DOI: http://dx.doi.org/10.2138/am-2017-6011

Figure 8

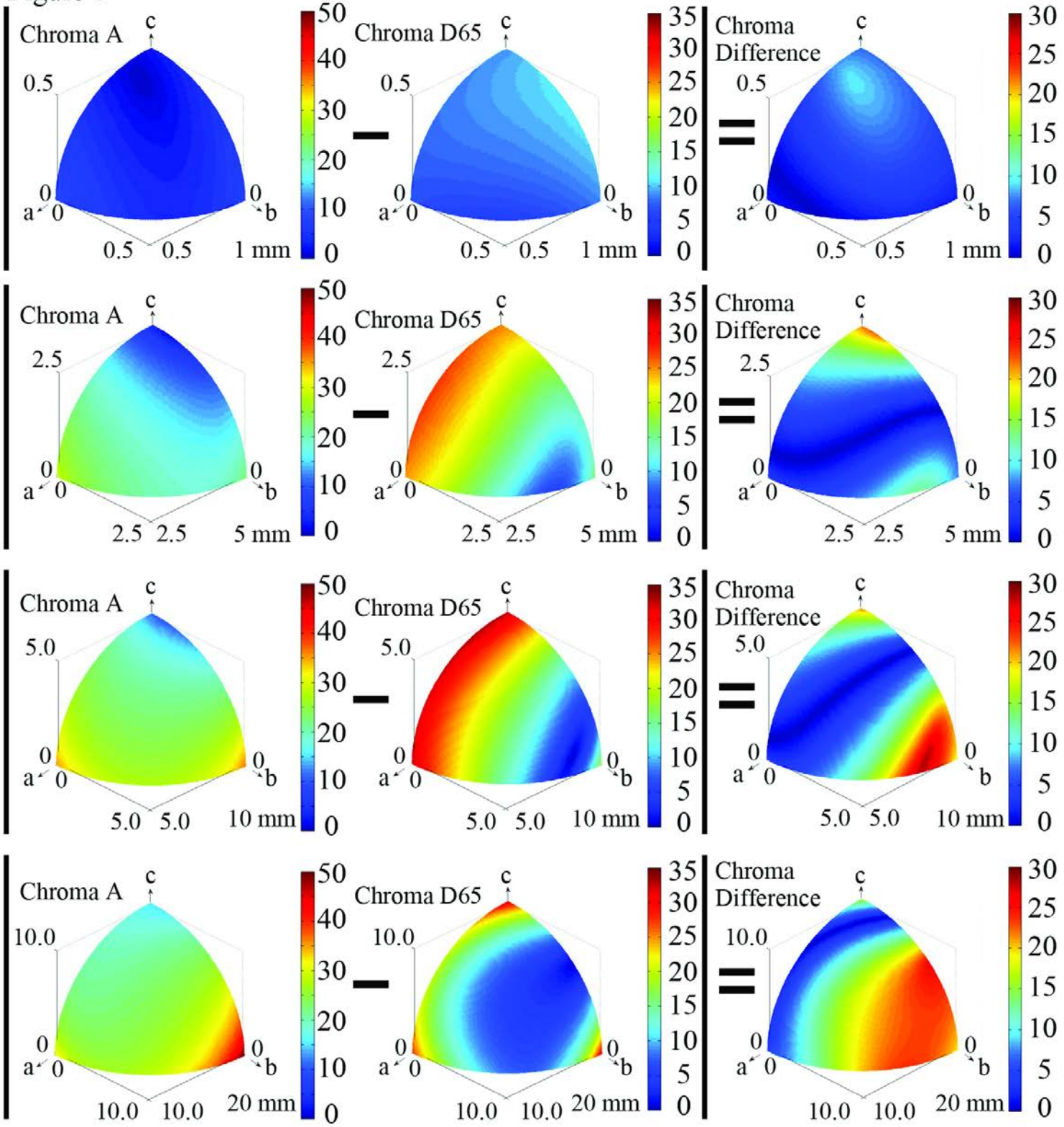

This is a preprint, the final version is subject to change, of the American Mineralogist (MSA)
Cite as Authors (Year) Title. American Mineralogist, in press.
(DOI will not work until issue is live.) DOI: http://dx.doi.org/10.2138/am-2017-6011

Figure 9

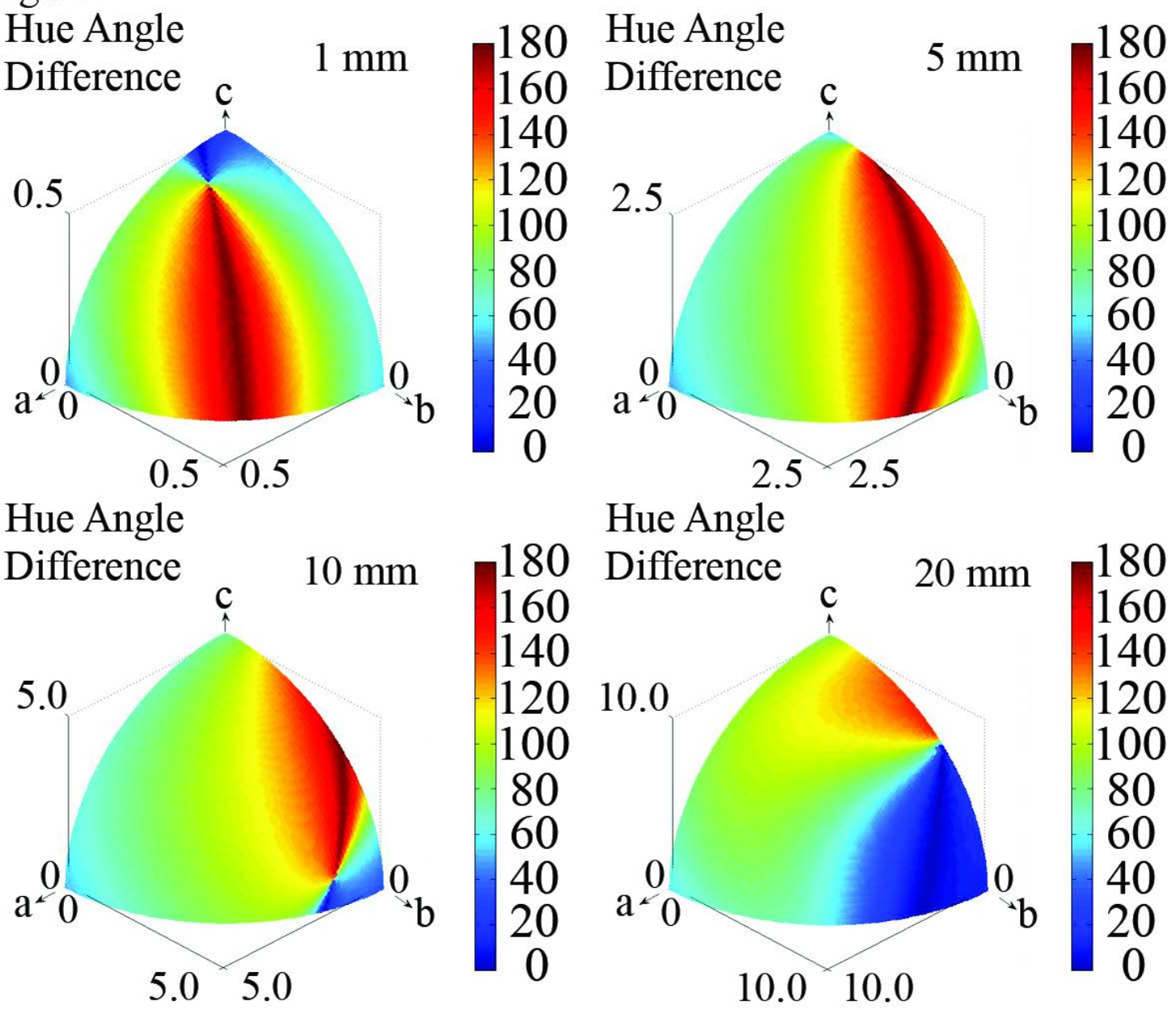

This is a preprint, the final version is subject to change, of the American Mineralogist (MSA)
Cite as Authors (Year) Title. American Mineralogist, in press.
(DOI will not work until issue is live.) DOI: http://dx.doi.org/10.2138/am-2017-6011

Figure 10

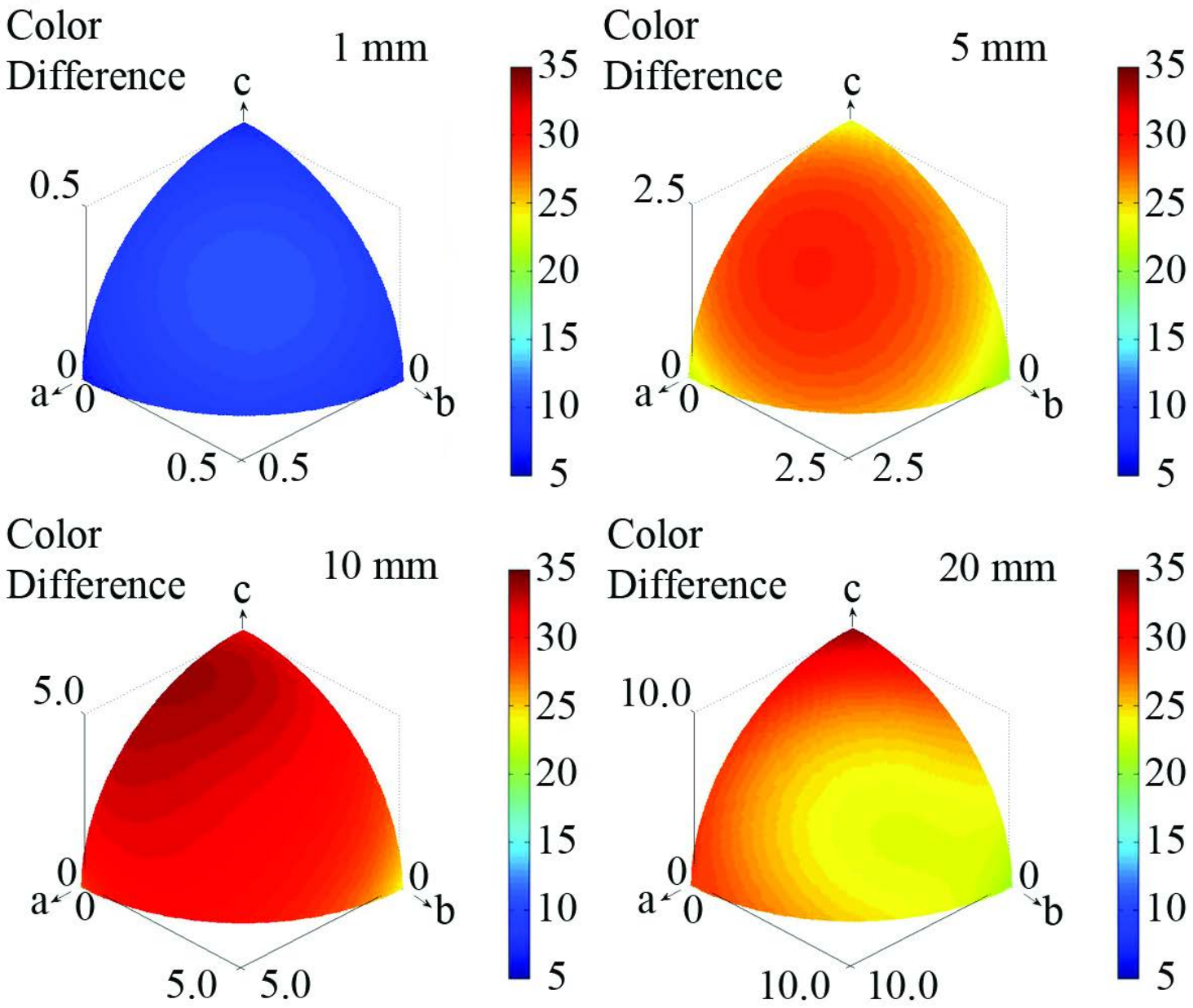

This is a preprint, the final version is subject to change, of the American Mineralogist (MSA)
Cite as Authors (Year) Title. American Mineralogist, in press.
(DOI will not work until issue is live.) DOI: http://dx.doi.org/10.2138/am-2017-6011

Figure 11

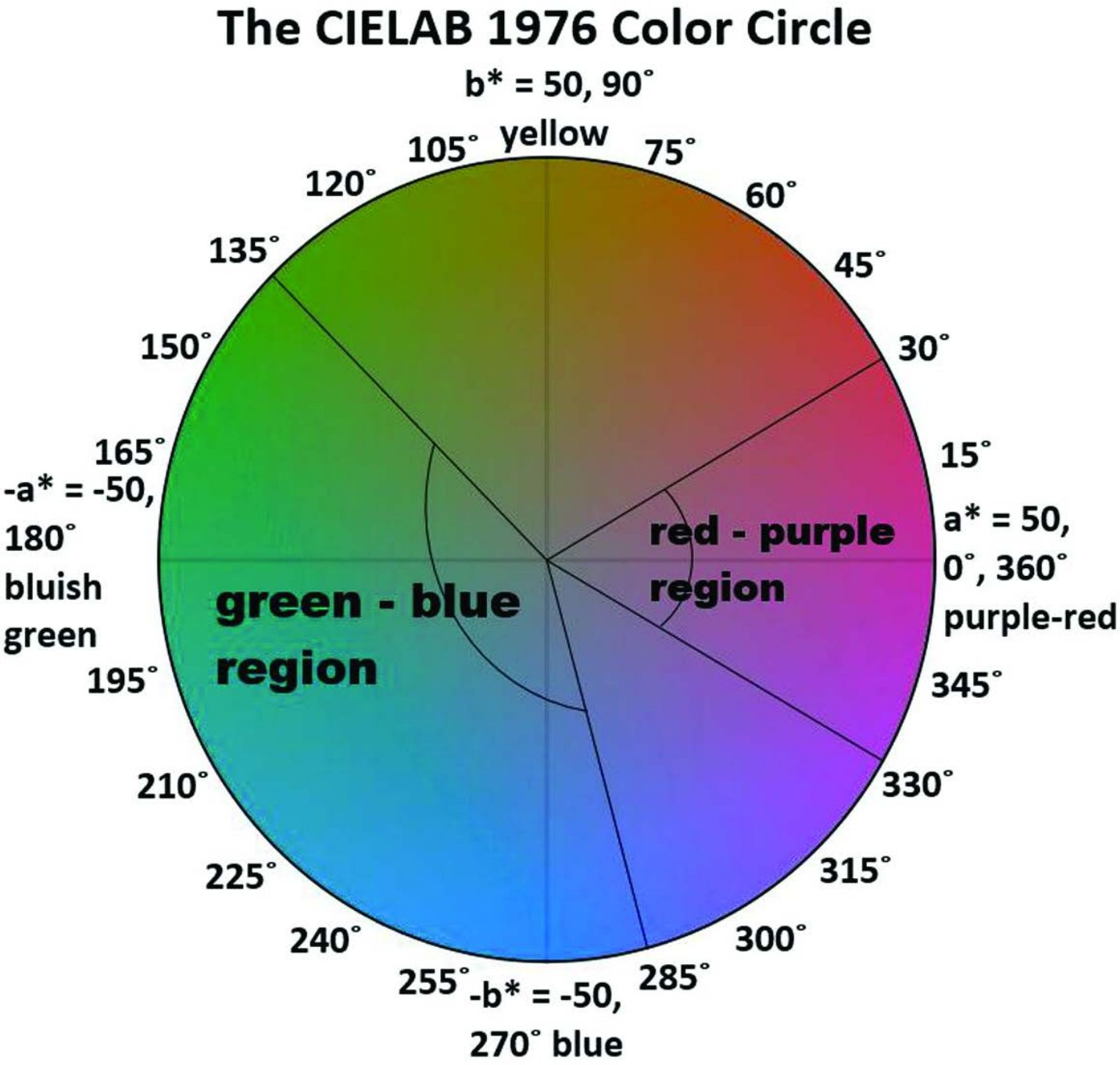

This is a preprint, the final version is subject to change, of the American Mineralogist (MSA)
Cite as Authors (Year) Title. American Mineralogist, in press.
(DOI will not work until issue is live.) DOI: http://dx.doi.org/10.2138/am-2017-6011

Figure 12

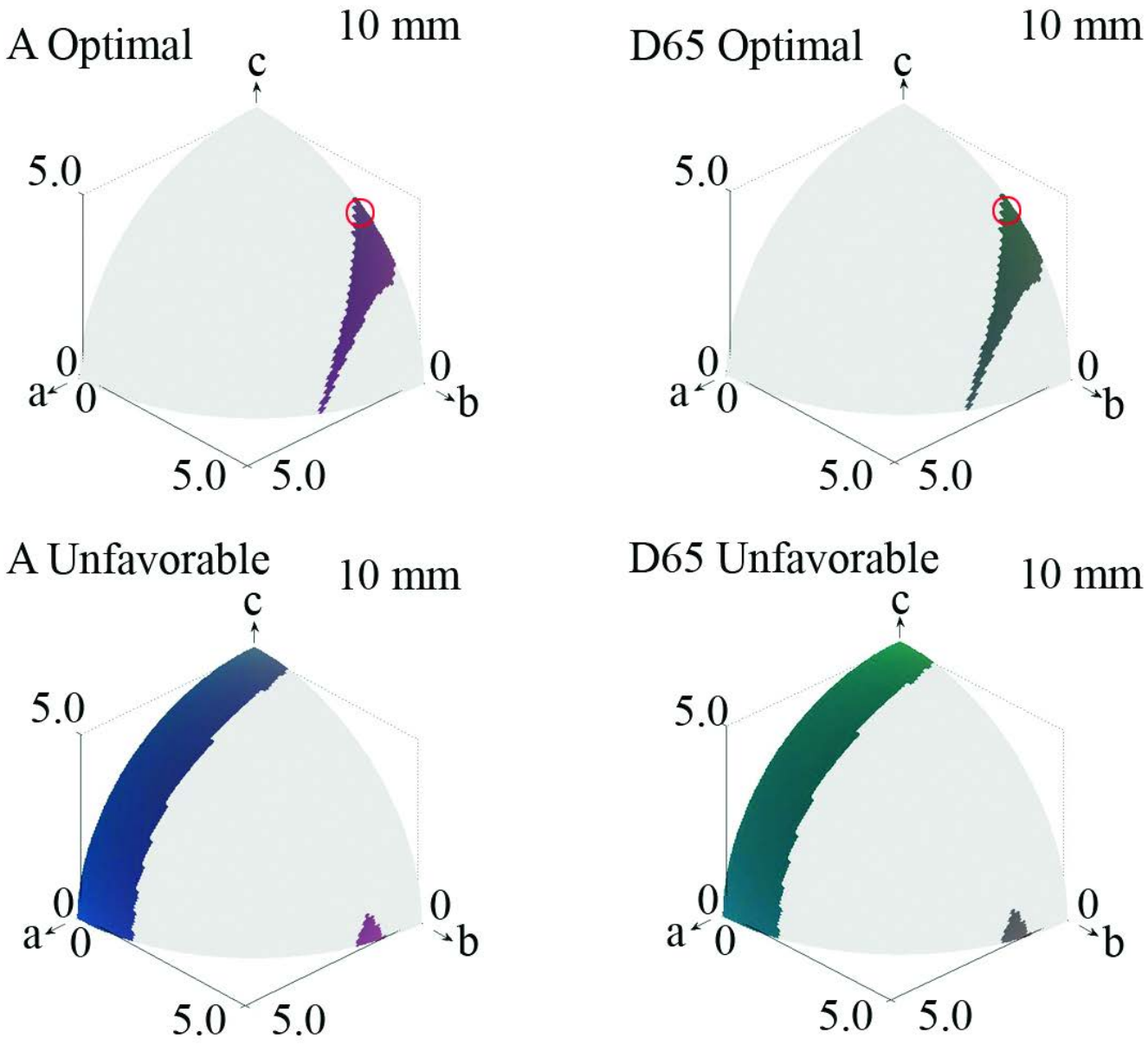

This is a preprint, the final version is subject to change, of the American Mineralogist (MSA)
Cite as Authors (Year) Title. American Mineralogist, in press.
(DOI will not work until issue is live.) DOI: http://dx.doi.org/10.2138/am-2017-6011

Figure 13

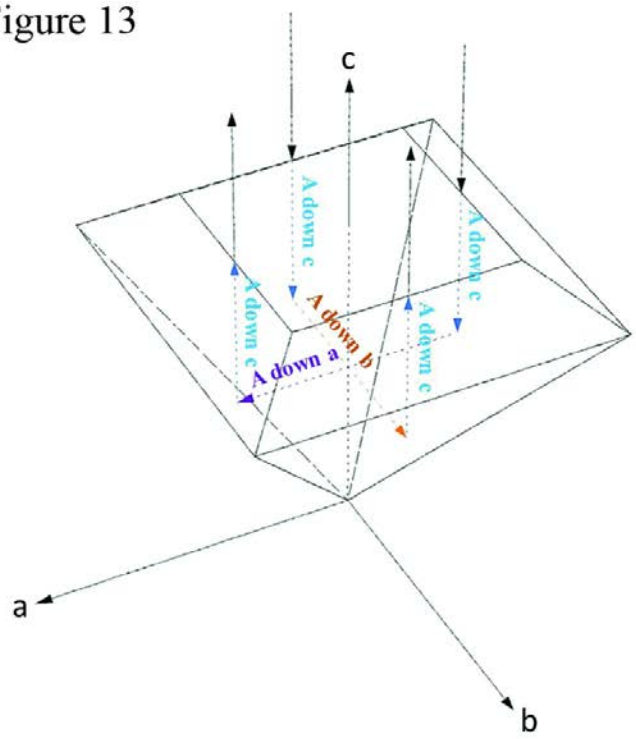

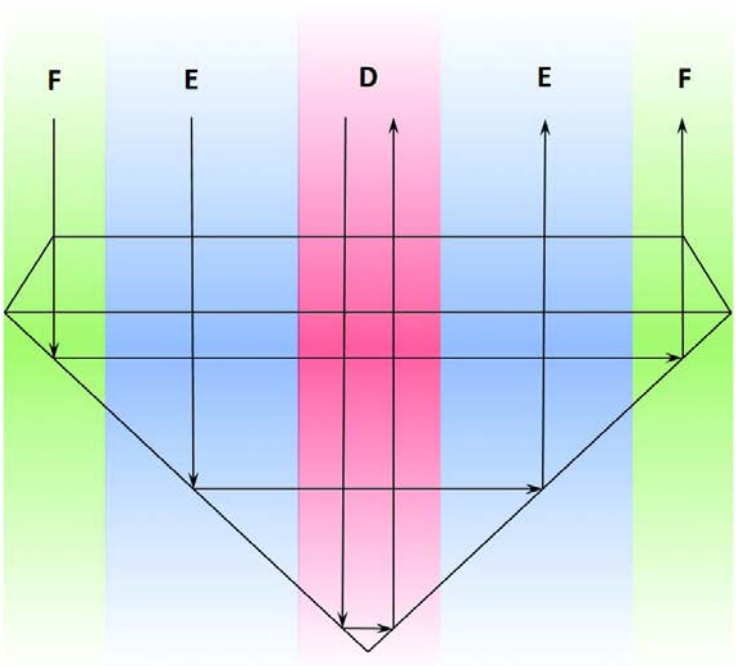

This is a preprint, the final version is subject to change, of the American Mineralogist (MSA)
Cite as Authors (Year) Title. American Mineralogist, in press.
(DOI will not work until issue is live.) DOI: http://dx.doi.org/10.2138/am-2017-6011

Figure 14

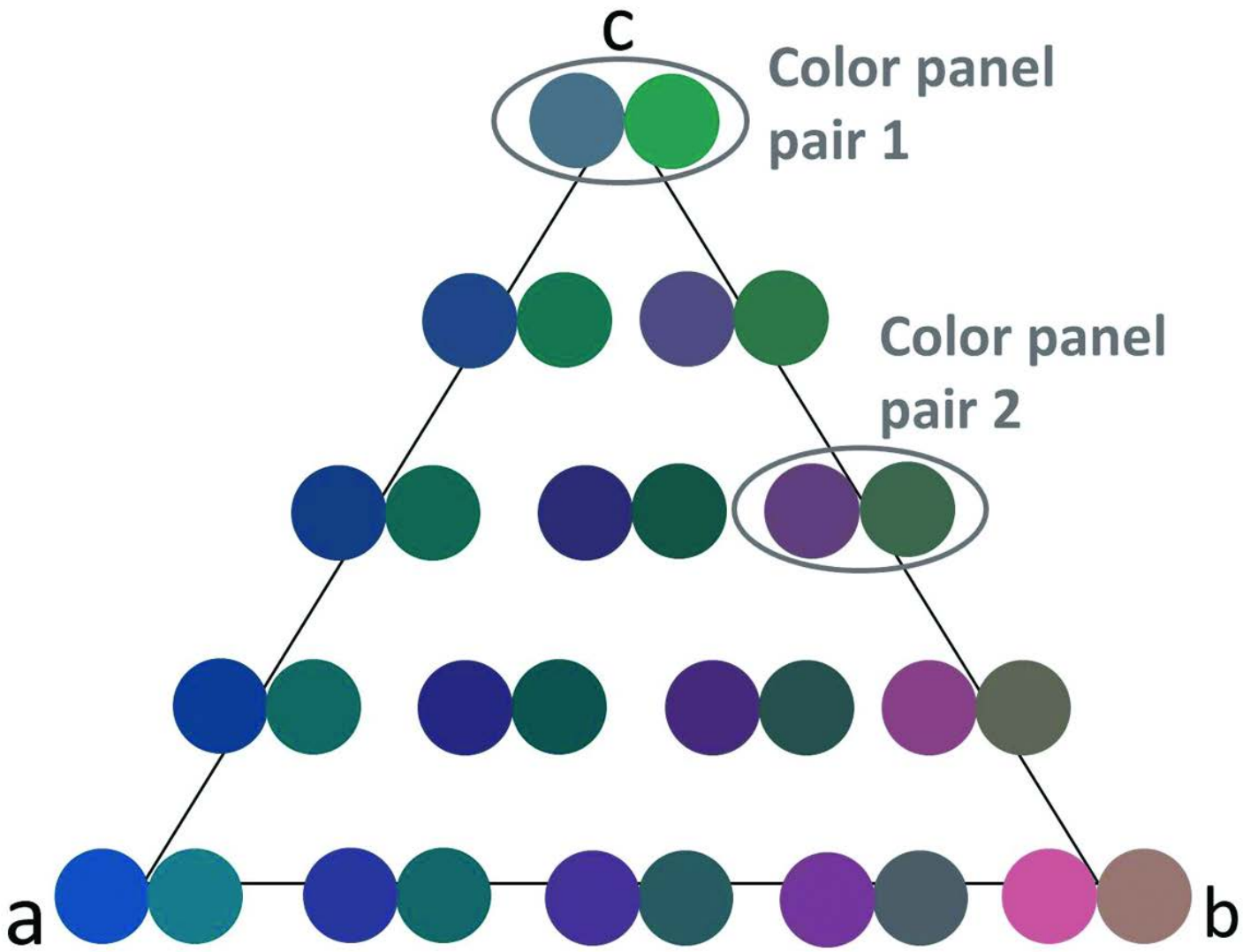

This is a preprint, the final version is subject to change, of the American Mineralogist (MSA)
Cite as Authors (Year) Title. American Mineralogist, in press.
(DOI will not work until issue is live.) DOI: http://dx.doi.org/10.2138/am-2017-6011

Figure 15